conformation, and makes the same interactions with the RNAP active-center "i" and "i + 1" sites, as in an elongation complex (Fig. 4A). The downstream dsDNA and the ribonucleotide primer GpA in the structures also exhibit the same conformations and interactions as the downstream dsDNA and the 3′ ribonucleotides of the RNA product in an elongation complex (Fig. 4A). We conclude that a promoter-dependent, initiation-factor–dependent transcription initiation complex is preorganized to proceed to transcription elongation without major changes in the conformation or interactions of the transcription-bubble template strand, downstream dsDNA, and RNA. The preorganization of the template strand in the promoter-dependent, initiation-factor–dependent initiation complex is in contrast to the situation in promoter-independent, initiation-factor–independent initiation complexes, in which template-strand ssDNA is disordered (*24*), or all but 5 nt of template-strand ssDNA is disordered (*25*), except in the presence of ≥4 nt of RNA. The presence of the initiation factor appears to account for the difference. The initiation factor σ makes direct interactions with the template strand that preorganize the template strand. The segment of σ region 3.2 (σR3.2) comprising σ residues 510 to 522—the "σ finger"—penetrates the RNAP active-center cleft, occupies part of the region occupied by RNA in a transcription elongation complex, makes an aromatic-amino-acid/base edge-edge interaction with the template-strand base at position –4, and makes four H bonds with Watson-Crick atoms of the template-strand bases at positions –4 and –3 (Fig. 4B and fig. S11). The interactions with DNA bases at template-strand positions –4 and –3 involve σ residues D514, D516, D517, and F522. Alanine substitutions of these residues result in defects in transcription (Fig. 4C). The interactions between the σ finger and the template strand constrain the template strand to adopt an A-form helical conformation and buttress the template strand to engage the RNAP active center in a manner compatible with binding of initiating NTPs. These interactions provide a structural explanation for the ability of the σ finger to facilitate the binding of initiating NTPs (*26*, *27*). The interactions between the σ finger and the template strand must be disrupted, and the σ finger must be displaced, to synthesize >4 nt of RNA. The need to disrupt these interactions and displace the σ finger provides a structural explanation for effects of the σ finger on abortive initiation (*26*, *27*).

The structures also define the conformational state of the RNAP clamp—the movable wall of the RNAP active-center cleft (*28*)—in the transcription initiation complex (Fig. 4, D and E). The clamp is closed by ~11° relative to the crystal structure of RNAP holoenzyme (Fig. 4D) and exhibits the same conformation as in the crystal structure of the elongation complex (Fig. 4E), consistent with fluorescence-resonance-energy-transfer results indicating that the clamp closes upon formation of RPo and remains closed during elongation (*28*). The finding that clamp conformations are the same in the initiation complex and the elongation complex provides further evidence that the initiation complex is preorganized to proceed to elongation.

The structures of RPo and RPo-GpA determined in this work reveal how RNAP and σ interact with the transcription-bubble nontemplate strand to accomplish promoter recognition and promoter unwinding and reveal how RNAP and σ interact with the transcription-bubble template strand and downstream dsDNA to preorganize the transcription initiation complex for subsequent reactions. The structures provide a foundation for understanding transcription initiation and transcriptional regulation.

References and Notes

1. R. M. Saecker, M. T. Record Jr., P. L. Dehaseth, *J. Mol. Biol.* **412**, 754 (2011).
2. N. Naryshkin, A. Revyakin, Y. Kim, V. Mekler, R. H. Ebright, *Cell* **101**, 601 (2000).
3. V. Mekler *et al*., *Cell* **108**, 599 (2002).
4. B. P. Hudson *et al*., *Proc. Natl. Acad. Sci. U.S.A.* **106**, 19830 (2009).
5. K. S. Murakami, S. Masuda, E. A. Campbell, O. Muzzin, S. A. Darst, *Science* **296**, 1285 (2002).
6. X. Liu, D. A. Bushnell, D. Wang, G. Calero, R. D. Kornberg, *Science* **327**, 206 (2010).
7. D. Kostrewa *et al*., *Nature* **462**, 323 (2009).
8. B. Treutlein *et al*., *Mol. Cell* **46**, 136 (2012).
9. S. Grünberg, L. Warfield, S. Hahn, *Nat. Struct. Mol. Biol.* **19**, 788 (2012).
10. Materials and methods are available as supplementary materials on *Science* Online.
11. R. Shultzaberger, Z. Chen, K. Lewis, T. Schneider, *Nucleic Acids Res.* **35**, 771 (2007).
12. A. Feklistov *et al*., *Mol. Cell* **23**, 97 (2006).
13. S. P. Haugen *et al*., *Cell* **125**, 1069 (2006).
14. V. Mekler, L. Minakhin, K. Severinov, *J. Biol. Chem.* **286**, 22600 (2011).
15. D. A. Siegele, J. C. Hu, W. A. Walter, C. A. Gross, *J. Mol. Biol.* **206**, 591 (1989).
16. C. Waldburger, T. Gardella, R. Wong, M. M. Susskind, *J. Mol. Biol.* **215**, 267 (1990).
17. A. Feklistov, S. A. Darst, *Cell* **147**, 1257 (2011).
18. X. Liu, D. A. Bushnell, R. D. Kornberg, *Cell* **147**, 1218 (2011).
19. S. P. Haugen, W. Ross, M. Manrique, R. L. Gourse, *Proc. Natl. Acad. Sci. U.S.A.* **105**, 3292 (2008).
20. A. C. Cheung, P. Cramer, *Nature* **471**, 249 (2011).
21. M. L. Kireeva, C. Domecq, B. Coulombe, Z. F. Burton, M. Kashlev, *J. Biol. Chem.* **286**, 30898 (2011).
22. P. P. Hein, M. Palangat, R. Landick, *Biochemistry* **50**, 7002 (2011).
23. R. Landick, *Proc. Natl. Acad. Sci. U.S.A.* **106**, 8797 (2009).
24. X. Liu, D. A. Bushnell, D. A. Silva, X. Huang, R. D. Kornberg, *Science* **333**, 633 (2011).
25. A. C. Cheung, S. Sainsbury, P. Cramer, *EMBO J.* **30**, 4755 (2011).
26. K. S. Murakami, S. Masuda, S. A. Darst, *Science* **296**, 1280 (2002).
27. A. Kulbachinskiy, A. Mustaev, *J. Biol. Chem.* **281**, 18273 (2006).
28. A. Chakraborty *et al*., *Science* **337**, 591 (2012).
29. D. G. Vassylyev, M. N. Vassylyeva, A. Perederina, T. H. Tahirov, I. Artsimovitch, *Nature* **448**, 157 (2007).
30. D. G. Vassylyev *et al*., *Nature* **417**, 712 (2002).

Acknowledgments: We thank the Brookhaven National Synchrotron Light Source and Cornell High Energy Synchrotron Source for beamline access; the Argonne Photon Source CCP4 School for training; and S. Borukhov, P. deHaseth, K. Kuznedelov, L. Minakhin, K. Severinov, and D. Temiakov for plasmids and discussion. This work was funded by NIH grants GM41376 and AI072766 and a Howard Hughes Medical Institute Investigatorship to R.H.E. PDB accession codes are 4G7H, 4G7Z, and 4G7O.

Supplementary Materials

www.sciencemag.org/cgi/content/full/science.1227786/DC1
Materials and Methods
Figs. S1 to S11
References (*31*–*48*)

23 July 2012; accepted 26 September 2012
Published online 18 October 2012;
10.1126/science.1227786

Dedifferentiation of Neurons and Astrocytes by Oncogenes Can Induce Gliomas in Mice

Dinorah Friedmann-Morvinski,[1] Eric A. Bushong,[2] Eugene Ke,[1,3] Yasushi Soda,[1] Tomotoshi Marumoto,[1,4] Oded Singer,[1] Mark H. Ellisman,[2] Inder M. Verma[1]*

Glioblastoma multiforme (GBM) is the most common and aggressive malignant primary brain tumor in humans. Here we show that gliomas can originate from differentiated cells in the central nervous system (CNS), including cortical neurons. Transduction by oncogenic lentiviral vectors of neural stem cells (NSCs), astrocytes, or even mature neurons in the brains of mice can give rise to malignant gliomas. All the tumors, irrespective of the site of lentiviral vector injection (the initiating population), shared common features of high expression of stem or progenitor markers and low expression of differentiation markers. Microarray analysis revealed that tumors of astrocytic and neuronal origin match the mesenchymal GBM subtype. We propose that most differentiated cells in the CNS upon defined genetic alterations undergo dedifferentiation to generate a NSC or progenitor state to initiate and maintain the tumor progression, as well as to give rise to the heterogeneous populations observed in malignant gliomas.

Despite progress in the genetic analysis and classification of gliomas based on pathology and genomics, the prognosis for patients with brain tumors continues to be very poor (*1*). One of the reasons for the lack of clinical advances in the treatment of glioblastoma

multiforme (GBM) for decades has been the insufficient understanding of the underlying mechanisms of progression and recurrence of gliomagenesis.

We recently used Cre-inducible lentiviral vectors to generate a novel mouse glioma model (*2*). Here we have expanded the utility of our lentiviral system by generating a new construct that carries two short hairpin RNAs (shRNAs): one targeting the gene encoding neurofibromatosis type I (NF1, mutated in 18% of GBMs) and the other targeting p53 (mutated in over 35% of GBMs) (Fig. 1, A and B). It has previously been shown that the combined loss of both NF1 and p53 results in high-grade glioma formation (*3*, *4*). The loss of NF1 leads to increased Ras mitogenic signaling and augments cell proliferation, whereas the loss of functional p53 induces genomic instability, two important events relevant for tumorigenesis that were part of our rationale for using H-RasV12 and the inactivation of p53 in the initial pTomo lentivector (*2*).

[1]Laboratory of Genetics, The Salk Institute for Biological Studies, La Jolla, CA 92037, USA. [2]Center for Research in Biological Systems, National Center for Microscopy and Imaging Research, University of California San Diego, La Jolla, CA 92093, USA. [3]Graduate Program in Bioinformatics, University of California San Diego, La Jolla, CA 92093, USA. [4]Division of Molecular and Clinical Genetics, Department of Molecular Genetics, Medical Institute of Bioregulation, Kyushu University, Higashi-ku, Fukuoka 812-8582, Japan.

*To whom correspondence should be addressed. E-mail: verma@salk.edu

As shown in Fig. 1C and fig. S1, stereotaxic injection of oncogenic lentivector containing either shNF1-shp53 or H-RasV12-shp53 in the hippocampus (HP) of glial fibrillary acidic protein (GFAP)–Cre mice gives rise to gliomas with similar histological and morphological characteristics. Glial cells (*5*, *6*), oligodendrocyte precursor cells (*7*, *8*), and neural stem cells (NSCs) (*4*, *9*) have been suggested to be good candidates for the cell of origin of gliomas. Here we show that neurons can also be the target of transformation and generate malignant gliomas. Injections of shNF1-shp53 virus in the cortex (CTX) of Synapsin I-Cre transgenic mice (SynI-Cre; 8 to 16 weeks old), which express Cre specifically in neurons but not in glial cells (*10*), induced the formation of gliomas (Fig. 2A). Because the shRNAs targeting genes encoding either NF1 or p53 are not regulated by Cre (Fig. 1A), the tumors that we obtained were a mixture of green fluorescent protein–positive and red fluorescent protein–negative (GFP^+/RFP^-) or GFP^+/RFP^+ (due to leakiness from the internal ribosome entry site; see arrows in Fig. 2B). Only tumor cells that are GFP^+/RFP^- are considered to be of neuronal origin, because they are expressing Cre to delete RFP. We extended these results by transducing H-RasV12-p53 vector in the CTX of Syn1-Cre mice. Neurons transduced with this oncogenic vector expressed only GFP, because the expression of Ras is regulated by Cre (fig. S2) (*10*).

Analysis of brain sections 5 days after the injection of the lentivirus revealed GFP^+/RFP^- expression specifically in $NeuN^+$ and $Tuj1^+$ cells (see representative images in Fig. 2C and quantification of staining in table S1), and the same specificity was observed when SynI-Cre mice were crossed with a LacZ reporter line (fig. S3A), both results showing that Cre is specifically expressed in terminally differentiated neurons (*10*). To provide further evidence that mature neurons can be transformed by these oncogene/tumor suppressor genes as observed in vivo, we isolated primary cortical neurons from SynI-Cre mice and transduced them in vitro with shNF1-shp53 virus. The isolated neurons were Map2-positive (a marker of mature neurons), GFAP-negative, doublecortin-negative (a neuronal progenitor marker), and Ki67-negative (a marker for cell proliferation) (figs. S4A and S5). The transduced neurons were transplanted into NOD-SCID mice, and the resulting tumors (fig. S4B) exhibited the same histopathology features as those observed with the direct in vivo stereotaxic transductions. These tumors also expressed high levels of the progenitor markers Nestin and Sox2 (fig. S4C).

To determine the frequency of the tumor-initiating cells in tumors obtained by shNF1-shp53 injections in the CTX of SynI-Cre mice, we dissociated the tumors in single-cell suspension and sorted them into two different populations: GFP^+/RFP^- and GFP^+/RFP^+ cells. After limiting dilution analysis, we transplanted these cells back into new mice and obtained in both cases and with similar frequencies high-grade

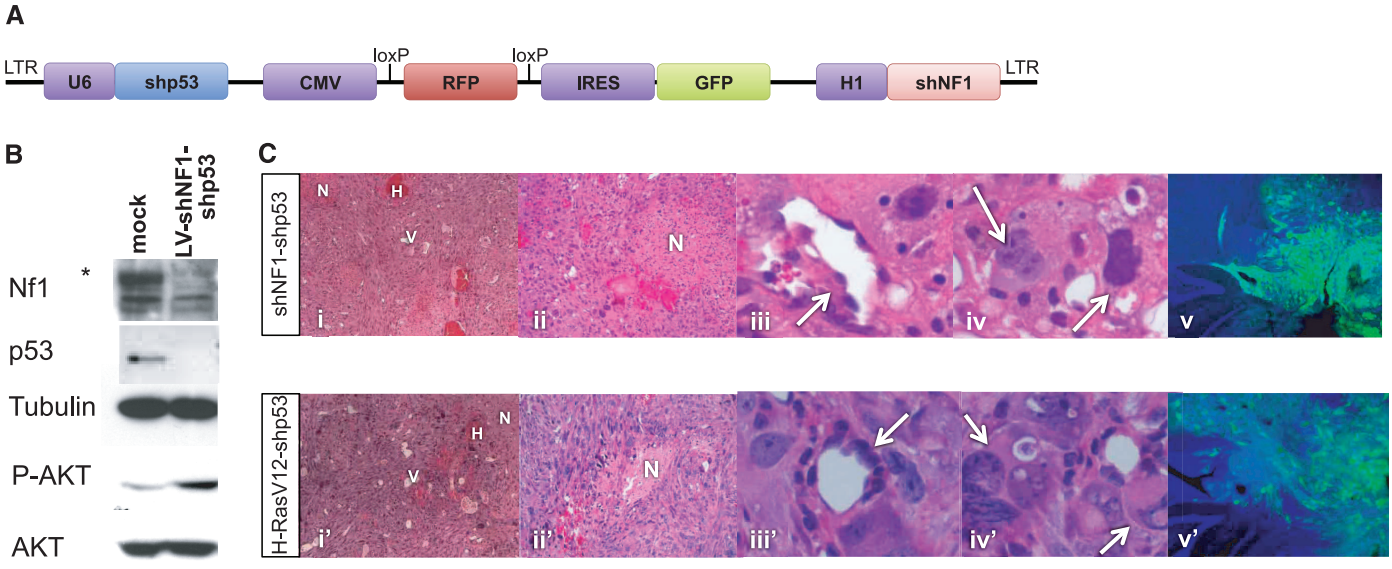

Fig. 1. Glioblastomas induced by a single lentiviral vector. (**A**) Schematic representation of the lentivector. In the shNF1-shp53 vector, the hairpin targeting NF1 was cloned under the H1 promoter at the 3′ untranslated region, and the hairpin targeting p53 was cloned 5′ to the cytomegalovirus promoter and under the U6 promoter. LTR, long terminal repeat. (**B**) Western blot (WB) showing silencing of both NF1 and p53. NF1 loss resulted in increased phosphorylation of Akt (P-Akt); total Akt expression was used as a control. MEF/$Ikk2^{-/-}$ cells were infected with the indicated lentivectors. The cell lysate was collected and analyzed by WB. Tubulin detection was used as a loading control. (**C**) Hematoxylin and eosin (H&E) histology and immunofluorescence of sections from either shNF1-shp53– or H-RasV12-shp53–induced glioblastomas in GFAP-Cre mice (HP injected). (i) and (i′) show images of the tumors (magnification ×20), in which increased cellularity, vascularity (V), hemorrhage (H), and necrotic areas (N) can be observed. The rest of the panels show all the classical GBM features: necrotic areas [N, (ii) and (ii′); ×40), perivascular infiltration [indicated by arrows in (iii) and (iii′); ×40 plus two electrical zoom], and multinucleated giant cells [arrows in (iv) and (iv′); ×40 plus two electrical zoom]. (v) and (v′) show, by immunofluorescence staining, the infiltrative characteristic of the tumor, crossing the midline and migrating to the other hemisphere (blue, DAPI; green, GFP; ×5).

gliomas (fig. S4D). In culture, these cells present all the characteristics of tumor-initiating cells (fig. S6).

We also used a second transgenic model, CamK2a-Cre mice (*11*), to target mature neurons with our oncogenic lentivectors (figs. S3 and S7). Even though both SynI-Cre and CamK2a-Cre mice were injected using the same virus titer (1×10^9 infectious units), the latter developed tumors with a much longer latency. These results can be explained by the different subtypes of neurons that were targeted when the CamK2a-Cre mice were used, mostly excitatory neurons, which may be more refractory to transformation, in addition to being less numerous in the CTX (*11*).

In the central nervous system (CNS) of adult mice, constitutive neurogenesis is observed mainly in two regions: the subventricular zone (SVZ) and the subgranular zone (SGZ) of the HP (*1*, *12*). Glial-lineage progenitors have been found in areas outside the classic neurogenic regions, including the optic nerve, striatum, hypothalamus, and subcortical white matter, but in these areas the majority of cells expressing GFAP are mostly differentiated astrocytes (*13*). For the next series of injections, we elected to use the oncogenic vector H-RasV12-shp53, in which the oncogene is Cre-inducible (limitation with the shNF1-shp53 vector). Furthermore, at the gross histological and transcriptional level, the two oncogenic vectors exhibit similar characteristics (Fig. 1). All transduced GFAP-Cre mice developed tumors when injected either in the HP, SVZ, striatum, or CTX (table S2). When Nestin-Cre mice were injected, tumors were obtained only when the virus was injected in the HP (SGZ) and SVZ but not in the CTX or striatum, because Nestin-expressing neural progenitor/stem cells are infrequent in these locations (*4*). Similar results were obtained when Sox2-Cre mice were injected in the same locations (table S2). Taking advantage of the GFP reporter in our oncogenic vector, we decided to follow the kinetics of expression of some of these markers during tumor development. Five days after injection of the vector in the CTX of 8-week-old GFAP-Cre mice (Fig. 3A, approximately 60 cells were infected), GFP^+/RFP^- cells were negative for NeuN, Ki67, Nestin, Olig2, and Rip markers but positive for GFAP, suggesting that glial cells were transduced. Using high-resolution large-scale mosaic images (*14*), we analyzed the expression of GFAP and Nestin markers at 2, 4, and 8 weeks after injection of the oncogenic vector either in the CTX (Fig. 3B) or the HP (fig. S8, A and B) of GFAP-Cre mice. Already at the early stages of cell proliferation (tumor initiation), most of the GFP^+ cells tended to lose GFAP expression, and as tumor growth progressed, the GFAP expression was progressively diminished (Fig. 3B). On the other hand, Nestin expression that was hardly detectable in the transduced cells 5 days after injection (Fig. 3A) increased significantly as tumors developed (Fig. 3B). Most of the cells that expressed Nestin by 8 weeks after injection also expressed Sox2, another progenitor marker (fig. S8C). Using qRT-PCR, we observed an increase of more progenitor/stem cell markers (*15*) as the tumor progressed and the mice succumbed to the disease, as well as diminished expression of differentiation state markers (*16*) (fig. S9). We suggest that the mature/differentiated cell initially infected, in the process of transformation, acquires the capacity to dedifferentiate to a cell that has the attributes of a neuroprogenitor cell, which can then not only maintain its pluripotency

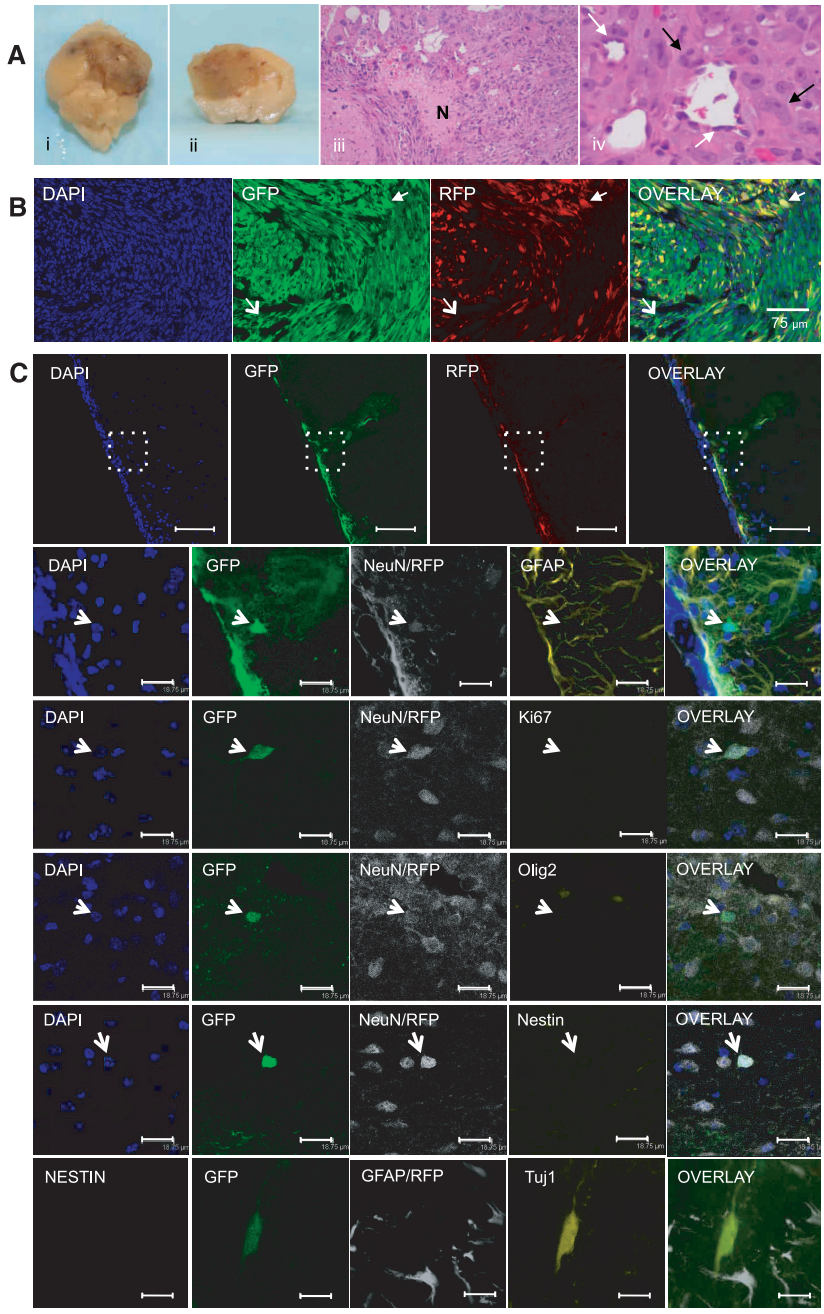

Fig. 2. Induction of gliomas by shNF1-shp53 lentiviral transduction of neurons. (**A**) Photographs (i) and (ii) showing the massive lesion in the brain and H&E staining of shNF1-shp53–induced tumors in the CTX of SynI-Cre mice [(iii), magnification ×40; (iv), magnification ×40 plus two electrical zoom, showing perivascular infiltration (white arrows) and a multinucleated giant cell (black arrows)]. (**B**) Confocal images showing the presence of both GFP^+/RFP^- (open arrowhead) and GFP^+/RFP^+ cells (solid arrowhead) in the tumor. (**C**) Confocal images showing oncogene/tumor suppressor expression specifically in $NeuN^+$ and $Tuj1^+$ cells. Five days after injection of the virus in the CTX of SynI-Cre transgenic mice, brains were collected and fixed. Sections of the brain were stained with the indicated antibodies. The upper panels show representative confocal images of GFP/RFP before antibody staining (scale bar, 75 μm). The lower panels show representative (arrows) colabeling using the antibodies/markers indicated in each panel. When possible, DAPI staining was also assessed (in blue). Scale bars, 18.75 μm; N, necrosis.

but also give rise to the heterogeneous cell populations observed in malignant gliomas (*2*).

To further confirm this hypothesis and support our in vivo observations, we established primary cortical astrocytes cultures from GFAP-Cre P11 (postnatal day 11) mice. These cells were characterized by immunofluorescent staining, expressed only bonafide markers of astrocytes (S-100β, GFAP-positive; Fig. 4A, panels ii to iv), and were Nestin and Sox2–negative (Fig. 4A, panel v). Early-passage $GFAP^+$ primary astrocytes (that expressed Cre as shown in Fig. 4A, panel vi, and were Ki67-negative as shown in fig. S5) were transduced in vitro with either shNF1-shp53 or H-RasV12-shp53 virus (fig. S10A, see expression of GFP; the efficiency of transduction was usually more than 90%) and transplanted into the brains of NOD-SCID mice (3×10^5 cells per injection). All the transplanted mice developed tumors with clinical and histopathological features (Fig. 4B) that were similar to those observed in the tumors obtained in the lentivirus-induced model (Fig. 1). Confocal microscopy analysis of these tumors revealed that the vast majority of the tumor cells (GFP^+) express progenitor markers Nestin and Sox2 (fig. S10B), and a few cells express Tuj1 (a neuronal marker) (see arrows in Fig. 4B). These findings further support the idea that terminally differentiated astrocytes can give rise to tumors that are composed of some differentiated neurons, thus providing evidence that these astrocytes underwent dedifferentiation (or possibly transdifferentiation) during tumorigenesis.

To mimic this dedifferentiation process in vitro, we took the shNF1-shp53– or H-RasV12-shp53–infected cortical astrocytes that were generated in media containing serum (under this condition, the cells maintained their astrocyte identity; Fig. 4C, panel i) and transferred them to stem cell media devoid of serum and supplemented with FGF-2. Under these new conditions, the cells started to change morphology, from a more elongated shape to a contracted cytoplasm, and in a time period of approximately 1 week, in the center of each aggregate of cells a small neurosphere-like structure formed and detached from the dish (Fig. 4C, panels ii to iv). These neurospheres, when collected from the supernatant, treated with low-grade trypsin (TrypLE), and cultured back in new dishes, continued to proliferate. These neurospheres showed expression of Nestin and Sox2 (Fig. 4D). Under the same tissue culture conditions, uninfected primary cortical astrocytes never changed their morphology and continued to retain the immunofluorescent markers of fully differentiated astrocytes (fig. S11, A and B). Primary astrocytes infected with a lentivirus containing only the shRNA targeting p53 or expressing only H-RasV12 (fig. S11, C and D) remained astrocytes. Our data support the notion that the cooperation between p53 deficiency and the receptor tyrosine kinase signaling pathway (through Ras activation) are both required for the dedifferentiation of astrocytes during tumorigenesis. Similarly, transduced mature neurons in vitro, when switched to NSC media supplemented with FGF-2, followed the same dedifferentiation changes as observed in the experiments described above using astrocytes and also formed neurosphere-like structures (fig. S12).

We performed qRT-PCR analysis to show that the dedifferentiated GFP^+ NSCs acquired the expression of NSC-specific genes and largely lost the astrocyte-specific genes (fig. S13). These GFP^+ NSCs also expressed CD133, a marker previously associated with brain cancer stem cells (*17*) (fig. S14A). These cells also expressed CD15, better known as SSEA1, a glycoprotein usually expressed in embryonic stem cells and commonly used for induced pluripotent stem (iPS) cell characterization (*18*) (fig. S14A). This was not the only common feature that we found our dedifferentiated GFP^+ NSCs share with reprogramming of normal iPS cells; the GFP^+ NSCs also express the transcription factors Sox2, c-myc, and Nanog and have an open, more relaxed chromatin structure (fig. S14, B and C).

Finally, the human relevance of our findings was supported by microarray analysis, which revealed that tumors derived from GFAP-Cre mice injected either in the CTX, HP, or SVZ, as well as tumors derived from SynI-Cre mice injected in the CTX, exhibit a very strong mesenchymal molecular subtype signature, whereas most of the Nestin Cre-derived tumors display a neural

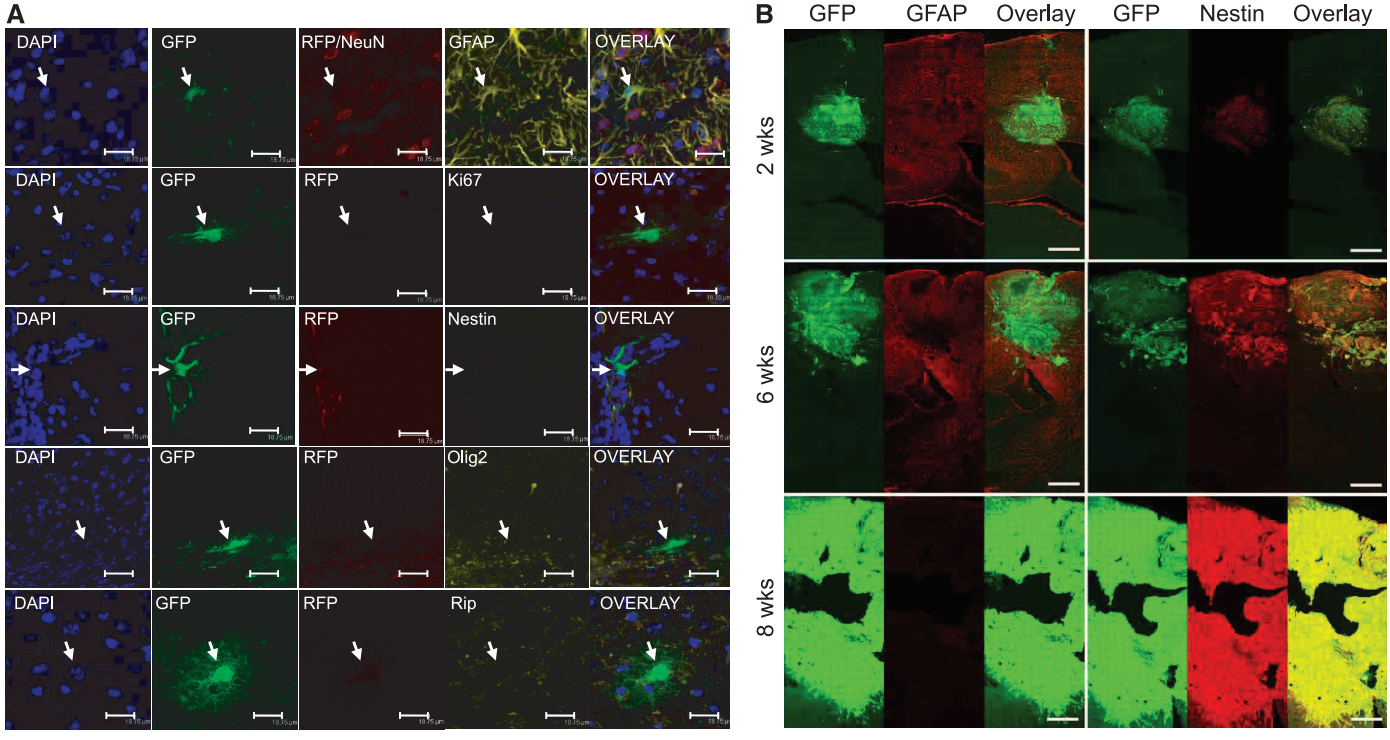

Fig. 3. Tumorigenesis in the CTX. (**A**) Confocal microscopy analysis of brain sections 5 days after injection of H-RasV12-shp53 virus in the CTX of GFAP-Cre mouse. Panels show representative (arrows) colabeling with the markers indicated in each of the images. Scale bars, 18.75 μm. (**B**) Maximum-intensity projections of large-scale mosaic volumes. Immunolabeling for GFAP and Nestin in tumors at 2, 6, and 8 weeks after the injection of lentivirus in the CTX is shown. GFAP staining intensity is seen to decrease with tumor progression, whereas Nestin labeling increases. Scale bars, 500 μm.

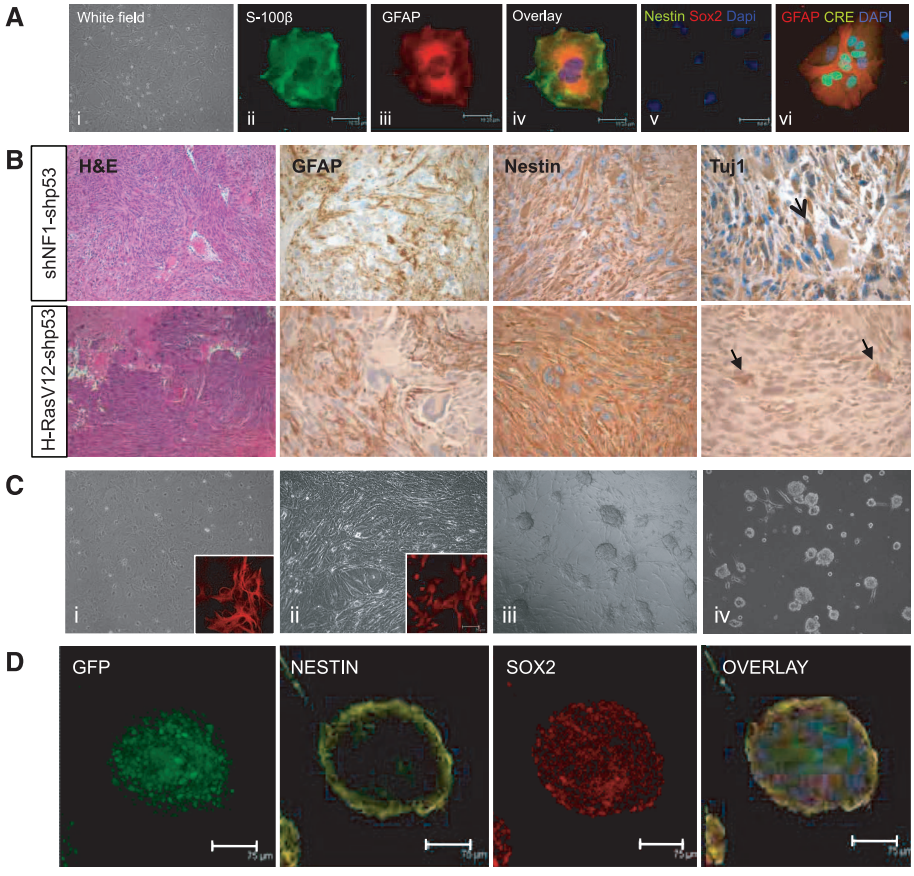

Fig. 4. Mature astrocytes transduced with either shNF1-shp53 or H-RasV12-shp53 virus dedifferentiate to a neural progenitor/stem cell–like state. (**A**) Morphology and staining of cortical astrocytes obtained from GFAP-Cre mice. Confocal microscopy analysis shows double staining for S-100β and GFAP (ii) to (iv), lack of expression of the stem/progenitor markers Nestin and Sox2 (v), and expression of Cre in all GFAP$^+$ astrocytes [(vi): red, GFAP; green, Cre; blue, DAPI]. (**B**) Tumors derived from either shNF1-shp53– or H-RasV12-shp53–transduced astrocytes orthotopically transplanted into the HP of NOD-SCID mice; H&E histology and immunohistochemistry. Arrows point to representative Tuj1-positive cells. (**C**) (i) Astrocytes before transduction maintained in media plus serum express GFAP (inset red, GFAP; scale bar, 75 μm). (ii) Transduced astrocytes in media plus serum (inset red, GFAP). (iii) and (iv) Transduced astrocytes transferred to serum-free media supplemented with FGF-2. Light microscopy magnification, ×20. (**D**) Confocal microscopy analysis of the neurospheres described in (C), (iv) [green, GFP (vector); yellow, Nestin; red, Sox2; scale bar, 75 μm].

subclass (fig. S15, A and B, and database S1). These results support our observations that both astrocytic- and neuronal-derived tumors not only have overlapping histopathological features but also share the same molecular signature. Our mouse model of GBM resembles the mesenchymal subtype, which is of high interest to the field, because patients having this classification exhibit worse survival and are more resistant to treatment than the other groups (*19*–*21*). The mesenchymal subtype is reminiscent of a transition that has been linked to dedifferentiated and transdifferentiated tumors (*22*), whereas the neural subtype is most similar to normal brain tissue, and its signature reflects a tendency to the differentiation phenotype (*23*). Finally, the The Cancer Genome Atlas study has revealed that both mesenchymal and neural subtypes harbor deletions and/or mutations in the NF1 and p53 genes (*23*), further supporting our findings that H-RasV12-shp53 tumors are representatives of the shNF1-shp53 tumors. Similar results were obtained when our microarray data were compared to the molecular signature identified by Phillips *et al*. (*20*) (fig. S15C).

We have shown that both NSCs residing either in the SVZ or HP (e.g., in Nestin-Cre– and Sox2-Cre–injected mice) and mature neurons and astrocytes can be targets of genetic alterations that can lead to gliomagenesis. Although we have not formally shown this using our lentiviral vectors system, it has already been reported that oligodendrocyte progenitor cells can also act as cells of origin for glioma (*7*, *8*). We propose that the genetically altered differentiated cell acquires the capacity to dedifferentiate to a more progenitor (stem cell) state, and that tumor progression probably requires a permissive microenvironment composed of cell types and molecular signals that can sustain both differentiation of tumor cells and the maintenance of tumor stem-like cells. Our results offer an explanation for the recurrence of gliomas after treatment, because any tumor cell that is not eradicated can continue to proliferate and induce tumor formation, thereby perpetuating the cycle of continuous cell replication to form malignant gliomas.

References and Notes

1. N. Sanai, A. Alvarez-Buylla, M. S. Berger, *N. Engl. J. Med.* **353**, 811 (2005).
2. T. Marumoto *et al*., *Nat. Med.* **15**, 110 (2009).
3. K. M. Reilly, D. A. Loisel, R. T. Bronson, M. E. McLaughlin, T. Jacks, *Nat. Genet.* **26**, 109 (2000).
4. S. Alcantara Llaguno *et al*., *Cancer Cell* **15**, 45 (2009).
5. H. Zhu *et al*., *Proc. Natl. Acad. Sci. U.S.A.* **106**, 2712 (2009).
6. L. M. Chow *et al*., *Cancer Cell* **19**, 305 (2011).
7. N. Lindberg, M. Kastemar, T. Olofsson, A. Smits, L. Uhrbom, *Oncogene* **28**, 2266 (2009).
8. C. Liu *et al*., *Cell* **146**, 209 (2011).
9. Y. Zhu *et al*., *Cancer Cell* **8**, 119 (2005).
10. Y. Zhu *et al*., *Genes Dev.* **15**, 859 (2001).
11. J. Z. Tsien *et al*., *Cell* **87**, 1317 (1996).
12. F. H. Gage, *Science* **287**, 1433 (2000).
13. J. Jiao, D. F. Chen, *Stem Cells* **26**, 1221 (2008).
14. D. L. Price *et al*., *Neuroinformatics* **4**, 65 (2006).
15. T. Hide *et al*., *Stem Cells* **29**, 590 (2011).
16. J. D. Cahoy *et al*., *J. Neurosci.* **28**, 264 (2008).
17. A. L. Vescovi, R. Galli, B. A. Reynolds, *Nat. Rev. Cancer* **6**, 425 (2006).
18. T. Brambrink *et al*., *Cell Stem Cell* **2**, 151 (2008).
19. C. E. Pelloski *et al*., *Clin. Cancer Res.* **11**, 3326 (2005).
20. H. S. Phillips *et al*., *Cancer Cell* **9**, 157 (2006).
21. H. Colman *et al*., *Neuro-oncol.* **12**, 49 (2010).
22. J. P. Thiery, *Nat. Rev. Cancer* **2**, 442 (2002).
23. R. G. Verhaak *et al*.; Cancer Genome Atlas Research Network, *Cancer Cell* **17**, 98 (2010).

Acknowledgments: We thank G. Estepa for her technical help, F. H. Gage and S. Subramaniam for useful discussions, and N. Varki and S. Kesari for pathological analysis. I.M.V. is an American Cancer Society Professor of Molecular Biology and holds the Irwin and Joan Jacobs Chair in Exemplary Life Sciences. D.F.-M. was supported by a fellowship from the European Molecular Biology Organization. This work was supported in part by grants from the National Institutes of Health (NIH) (HL053670), a Cancer Center Core Grant (P30 CA014195-38), Ipsen/Biomeasure, Sanofi Aventis, the H. N. and Frances C. Berger Foundation, and National Center for Research Resources grant 5P41RR004050 to M.H.E. The content is solely the responsibility of the authors and does not necessarily represent the official views of the National Institute of Allergy and Infectious Diseases or NIH. Microarray data have been deposited in the Gene Expression Omnibus (GEO) database (accession no. GSE35917). The authors (T.M., I.M.V., and Y.S.) and the Salk Institute have filed a patent application relating to mouse tumor models created with lentiviral vectors.

Supplementary Materials

www.sciencemag.org/cgi/content/full/science.1226929/DC1
Materials and Methods
Figs. S1 to S15
Tables S1 to S4
References (*24*–*34*)
Database S1

20 April 2012; accepted 21 September 2012
Published online 18 October 2012;
10.1126/science.1226929